

Article

Hierarchical Design of Homologous NiCoP/NF from Layered Double Hydroxides as a Long-Term Stable Electrocatalyst for Hydrogen Evolution

Shenglu Song¹, Ailing Song^{1,2,*} , Lei Bai¹, Manman Duanmu¹, Lixin Wang^{3,*}, Haifeng Dong^{1,*}, Xiujuan Qin¹ and Guangjie Shao^{1,2,*} 

- ¹ Hebei Key Laboratory of Applied Chemistry, College of Environmental and Chemical Engineering, Yanshan University, Qinhuangdao 066004, China; slsong@stumail.ysu.edu.cn (S.S.); bl0901@stumail.ysu.edu.cn (L.B.); manman.duanmu@stumail.ysu.edu.cn (M.D.); qinxj@ysu.edu.cn (X.Q.)
- ² State Key Laboratory of Metastable Materials Science and Technology, Yanshan University, Qinhuangdao 066004, China
- ³ Shijiazhuang Key Laboratory of Low Carbon Energy Materials, College of Chemical Engineering, Shijiazhuang University, Shijiazhuang 050035, China
- * Correspondence: ailing.song@ysu.edu.cn (A.S.); 1902003@sjzc.edu.cn (L.W.); hfdong@ysu.edu.cn (H.D.); shaoguangjie@ysu.edu.cn (G.S.)

Abstract: Ternary transition metal phosphides (TTMPs) with two-dimensional heterointerface and adjustable electronic structures have been widely studied in hydrogen evolution reactions (HER). However, single-phase TMPs often have inappropriate H* adsorption energy and electronic transfer efficiency in HER. Herein, we utilized the heterogeneity in the crystal structure to design an efficient and stable catalyst from the NiCoP nanowire@NiCoP nanosheet on nickel foam (NW-NiCoP@NS-NiCoP/NF) for HER. Layered double hydroxides (LDHs) with a heterogeneous matrix on crystal surfaces were grown under different reaction conditions, and non-metallic P was introduced by anion exchange to adjust the electronic structure of the transition metals. The hierarchical structure of homologous NiCoP/NF from the LDH allows for a larger surface area, which results in more active sites and improved gas diffusion. The optimized NW-NiCoP@NS-NiCoP/NF electrode exhibits excellent HER activity, with an overpotential of 144 mV, a Tafel slope of 84.2 mV dec⁻¹ at a current density of 100 mA cm⁻² and remarkable stability for more than 500 h in 1.0 M KOH electrolyte. This work provides ideas for elucidating the rational design of structural heterogeneity as an efficient electrocatalyst and the in situ construction of hierarchical structures.

Keywords: layered double hydroxides; transition metal phosphide; homologous material; hydrogen evolution; hierarchical structure



Citation: Song, S.; Song, A.; Bai, L.; Duanmu, M.; Wang, L.; Dong, H.; Qin, X.; Shao, G. Hierarchical Design of Homologous NiCoP/NF from Layered Double Hydroxides as a Long-Term Stable Electrocatalyst for Hydrogen Evolution. *Catalysts* **2023**, *13*, 1232. <https://doi.org/10.3390/catal13091232>

Academic Editors: Ioan-Cezar Marcu and Octavian Dumitru Pavel

Received: 17 July 2023

Revised: 8 August 2023

Accepted: 21 August 2023

Published: 23 August 2023



Copyright: © 2023 by the authors. Licensee MDPI, Basel, Switzerland. This article is an open access article distributed under the terms and conditions of the Creative Commons Attribution (CC BY) license (<https://creativecommons.org/licenses/by/4.0/>).

1. Introduction

With the increasing demand for energy, water splitting, as a representative of clean production capacity, has attracted more and more of researchers' attention. Among them, the hydrogen evolution reaction (HER), as the upper limit of water splitting reaction performance, has made great progress in various research directions [1]. However, the multi-step proton double-electron transfer in HER still limits its micro-reaction kinetics and hinders the smooth progress of energy conversion [2,3]. At present, the platinum-based catalyst with the best performance has the problems of low earth abundance and high cost, and there are still many obstacles to large-scale industrial production. Transition metal phosphides (TMPs) are expected to be alternatives for noble metal catalysts due to their good conductivity, easy heteroatom doping and rich chemical states [4–6]. However, the catalytic performance of single-phase TMPs is far inferior to that of noble metal catalysts due to the limited number of active sites and inappropriate electronic structure. Ternary transition

metal phosphides (NiCoP, NiFeP, CoFeP) exhibit excellent HER, OER and overall water-splitting properties due to their enhanced electronic conduction and bimetallic synergistic effect [7–9]. Among them, NiCoP has promising potential as a non-noble metal catalyst for HER. This is due to its ability to tune the chemical states of the Ni and Co double sites, which optimizes the acceptance position of the hydrogen intermediate. Additionally, the introduction of P as an electron donor regulates the electronic structure and hydrogen adsorption energy of the bimetal. This enhances the electron transfer level, making it an effective catalyst [10–12]. Numerous researchers have explored the potential of NiCoP and have enhanced its catalytic performance by incorporating elemental doping, interfacial engineering and structural nanosizing [13–16]. For example, Mu et al. constructed Ru-doped NiCoP nanoflowers on a nickel foam (NF) substrate, which only required overpotentials of 216 mV to afford 20 mA cm^{-2} for OER and 44 mV to afford 10 mA cm^{-2} for HER [17]. Chen et al. designed unique hollow nanostructures, rich micro/mesoporous channels and optimized nanoparticles [18]. At current densities of 10, 50 and 100 mA cm^{-2} , the HER potentials are -0.052 , -0.115 and -0.159 V , respectively. Jiang et al. adjusted the morphology and structure of the product by changing the calcination temperature, constructing a richer heterogeneous interface in the catalysts. The obtained Co/NiCoP catalyst displays a low Tafel slope of 84 mV dec^{-1} and an overpotential of 54 mV at a current density of 10 mA cm^{-2} [19].

Researchers often use various methods, such as constructing heterointerfaces or doping heteroatoms, to expose more active centers and achieve the flexible and adjustable electronic structures of the catalysts. Jeon et al. used continuous three-dimensional (3D) nanopatterning to synthesize Ni_2P -coated 3D Ni composite nanostructures with Cu atom-doped Ni_3N [20,21]. The prepared catalyst exhibits good HER performance due to the optimized Gibbs free energy of H^* (ΔG_{H^*}), fast electron transfer channels and highly exposed active sites. The heterogeneity of the crystal structure can produce a large number of homogeneous interfaces of different crystal planes of the same material; enhance the internal mass transfer and charge transfer of the material; and give full play to the inherent catalytic performance of the material [22–24]. In addition, regulating the reaction conditions and the number of auxiliary reagents can further construct the nanostructures of materials. Layered nanostructures are a good choice for catalysts. They can provide rich material diffusion channels, a large number of junction interfaces and an expanded catalytic surface area [25,26]. Abundant material diffusion channels and a large number of junction interfaces can accelerate the release of generated gas and promote mass transfer. The increased specific surface area and layered structure not only increase the number of active sites, allowing them to be fully exposed, but also accelerate the transmission of electrons. By controlling the reaction temperature of the two-step hydrothermal reaction, the optimal growth orientation of the crystal can be effectively controlled, and the addition of morphology regulators can also effectively adjust the micromorphology of the material. The composite 3D nanostructures of nanowires (NWs) [27,28], nanosheets (NSs) [29–31], nanotubes (NTs) [32–34], and layered double hydroxide (LDH) nanosheets, such as “wire-on-sheet” [35,36], “sheet-on-sheet” [37–39] and “sheet-on-tube” [40,41] can effectively combine the HER properties of the active sites in different components and enhance the stability of the electrode [42–44]. These establishments of hierarchical structures can leverage the combined advantages of different structures, accelerate the mass and charge transfer rate of materials and improve the mechanical stability and flexibility of materials.

Secondary chemical conversion of hierarchical nanostructures can be achieved through anion exchange technology. In this work, we report a two-step hydrothermal and subsequent phosphating method for the hierarchical design of a homologous NiCoP/NF electrode from LDH (NiCoP nanowire@NiCoP nanosheet on nickel foam, NW-NiCoP@NS-NiCoP/NF). As shown in Scheme 1, basic nickel–cobalt carbonate nanowire and nanosheet arrays were grown in situ on NF substrate through hydrothermal reactions at different temperatures. Subsequently, according to the anion exchange reaction mechanism, the

precursor was phosphated in situ by PH_3 gas decomposed from sodium hypophosphite at $300\text{ }^\circ\text{C}$ to obtain fully converted NiCoP. In the hydrothermal reaction process, due to the differences in hydrothermal temperature and time, the optimal growth of basic nickel–cobalt carbonate crystal surface is also different. The combination of basic nickel–cobalt carbonate with different crystal phases can create a large number of hierarchical interfaces, accelerating the process of charge and mass transfer. The subsequent phosphating operation not only maintained the original morphology characteristics of the catalyst but also further adjusted the electronic structure of the NiCo bimetal, achieving a better HER performance. As a result, the optimal NW-NiCoP@NS-NiCoP/NF-160 electrode exhibits excellent electrocatalytic performance with a low overpotential of 80 and 144 mV at 10 mA cm^{-2} and 100 mA cm^{-2} , respectively, and remarkable stability for more than 500 h in 1.0 M KOH electrolyte.



Scheme 1. Schematic illustration of the preparation procedures of the NiCoP@NiCoP/NF.

2. Results and Discussion

2.1. Subsection

2.1.1. Structural Characterization of the Catalyst

The catalyst morphology was characterized by field emission scanning electron microscopy (FESEM) and transmission electron microscopy (TEM). Figure 1a shows the morphology of flake NiCo-LDH after the first step of hydrothermal treatment. The diamond-shaped flake LDH with a thickness of about 100 nm provides a stable substrate for in situ growth of needle-like NiCo-carbonate hydroxide. After the second step of the hydrothermal treatment, the nanowire array continues to grow on the original structure, forming a multi-level structure of “wire-on-sheet”. At the initial stage of the phosphating treatment, the NiCo hydroxide will decompose into OH^- and CO_3^{2-} at high temperatures, and the PH_3 gas generated by the decomposition of NaH_2PO_2 will react with the NiCo metal sites to generate the corresponding bimetallic phosphide. The morphology obtained after anion exchange is shown in Figure 1b,c. As shown in Figure 1b, after secondary hydrothermal treatment, NiCo hydroxide nanowires with a diameter of about 150 nm were grown in situ on the surface of the NF based on the original nanosheets. Nanosheets and nanowires combine to form nanoflowers, which increase the surface area of the catalyst and expose more active sites, providing a good channel for the transfer of catalytic intermediates. The nanowire array has completely covered the nanosheets, and the micro-environment where the nanosheets and nanowires coexist can be seen in the TEM of Figure 1c. The TEM image of the NiCoP@NiCoP/NF-160 shows a good combination of nanosheets and nanowires (Figure 1c). The element mapping in Figure 1d–f show the uniform distribution of Ni, Co and P elements. We also prepared control samples for one-step hydrothermal phosphating. Figure S1a,b show the SEM images of NiCoP nanosheets and NiCoP nanowires obtained

through a one-step hydrothermal process, respectively. It can be seen that the NiCoP after one-step hydrothermal phosphating exhibits distinct sheet or wire structures, providing a foundation for the establishment of composite structures.

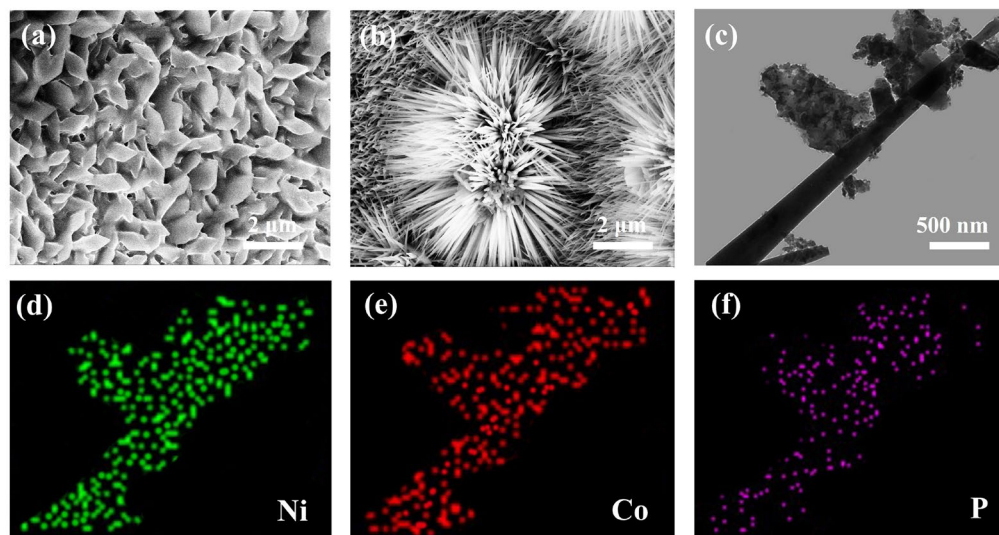


Figure 1. The SEM images of (a) NiCo-LDH/NF and (b) NiCoP@NiCoP/NF-160. (c) The TEM image of NiCoP@NiCoP/NF-160. (d–f) The elemental mapping images of the NiCoP@NiCoP/NF-160.

X-ray diffraction (XRD) and X-ray photoelectron spectroscopy (XPS) were used to investigate the structural transformation, electronic properties and valence states of the elements of NiCo phosphide produced by the two-step hydrothermal method. As shown in Figure S2—except that 44.5° , 51.8° and 76.4° correspond to the three strong peaks of Ni (111), (200) and (222) (PDF#87-0712) from NF substrate—the diffraction peaks at 41.0° , 44.9° , 47.6° and 54.4° correspond to the (111), (201), (210) and (300) crystal planes of NiCoP (PDF#71-2336), which prove that ternary NiCoP was successfully synthesized. Additionally, a clear splitting peak appeared at the Ni (222) diffraction peak corresponding to 76.4° , proving that Co atoms were doped into the Ni lattice [45]. Moreover, we found that NiCoP composite structures prepared at different hydrothermal temperatures in the second step exhibit different crystallinity. With the change of temperature and compared to the control samples, the diffraction peaks of NiCoP@NiCoP/NF-160 are intense and sharp, and there is no interference from impurity peaks, indicating that NiCoP@NiCoP/NF-160 has optimal crystallinity. The XPS spectra show that the surfaces of NiCoP@NiCoP/NF-160 (Figure 2a) and NiCoP/NF (Figure S3) both contain Ni, Co, P, C and O elements. The high-resolution Ni 2p XPS spectrum of NiCoP@NiCoP/NF-160 shows that there are two satellite peaks centered at 856.1 eV and 873.9 eV that can be designated as the characteristic spin orbit signals of Ni^{2+} (Figure 2b) [46]. The binding energy at 853.9 eV is assigned to Ni–P bonding [47]. Compared to NiCoP/NF, both peaks of Ni^{2+} 2p_{1/2} and 2p_{3/2} exhibit a negative shift of 0.4 eV. Similar analyses on Co 2p were performed, with three pairs of peaks corresponding to the Co–P, Co^{2+} and satellite peaks (Figure 2c). The peaks of Co–P and Co^{2+} of NiCoP@NiCoP/NF-160 also have a distinct shift toward low binding energy compared to the peaks in NiCoP/NF. The predominant peak at 133.5 eV could be ascribed to the P–O bonds, which resulted from the inevitable oxidation on the sample surface [48]. The positive shift of the P–O peak and the negative shift of the Ni^{2+} and Co^{2+} related peaks in NiCoP@NiCoP/NF-160 compared to NiCoP/NF proves that the composite structure of nanosheets and nanowires obtained after the two-step hydrothermal phosphitylation accelerates the charge transfer of the catalytic material and facilitates the redox reaction. Although XPS results suggest the presence of a small amount of nickel/cobalt phosphide in the sample, the XRD results indicate that the main component responsible for the catalytic role is the NiCoP phase.

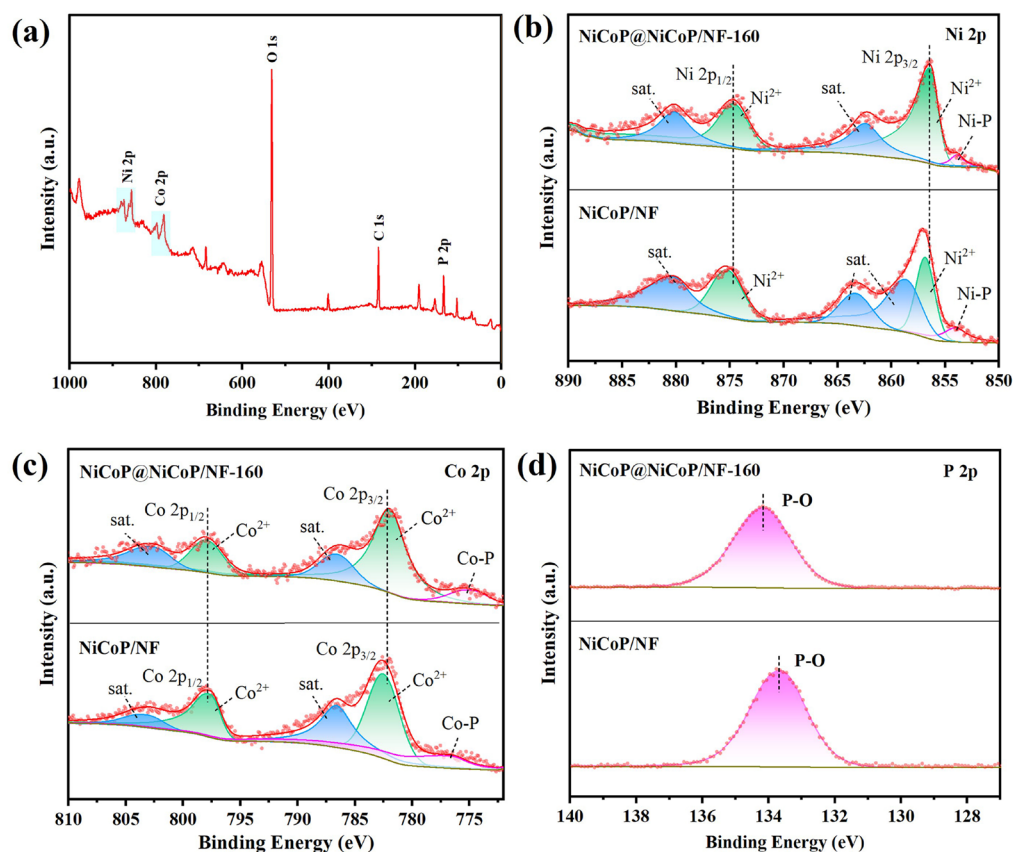


Figure 2. (a) XPS survey spectra of NiCoP@NiCoP/NF-160, high-resolution XPS spectra of (b) Ni 2p, (c) Co 2p and (d) P 2p of NiCoP@NiCoP/NF-160 and NiCoP/NF.

To optimize the nanowire shape of NiCoP@NiCoP/NF to achieve the optimal mass-transfer efficiency and accessible active sites, the effects of different hydrothermal temperatures on the size of the nanowires were recorded through SEM, TEM and XRD (Figure 3). With the continuous hydrothermal reaction, solute molecules will continue to destroy the solvation effect and overcome the formation of nuclear barriers by the crystals. The nucleation rate of crystals is related to the reaction temperature, and an increase in reaction temperature will accelerate the movement rate of solute molecules, thereby increasing the nucleation rate of crystals. At the same time as grain refinement, due to the existence of the Ostwald ripening effect, higher temperatures tend to promote grain growth and display different sizes of nanowires [49]. According to the TEM images in Figure 3d–f, as the hydrothermal temperature continues to rise, the morphology of the nanowire material changes from fine to dense at low temperatures and to coarse and sparse at high temperatures. Ultrafine nanowires can make the material unable to withstand the stress generated by bubble impact during the HER, leading to structural collapse and aggregation, which is particularly evident under reaction conditions of 120 °C. If the nanowire is too thick, it is not conducive to the effective exposure of the catalytic active site and the improvement of the electrochemical surface area, which affects the embodiment of catalytic activity. At a reaction temperature of 160 °C, mechanically stable nanowires were grown from the nanosheet structure, creating the best-graded structure. Appropriately sized nanowires increase the contact area with the electrolyte and the build mass and charge transfer channels from outside to inside, increasing the number of accessible active sites.

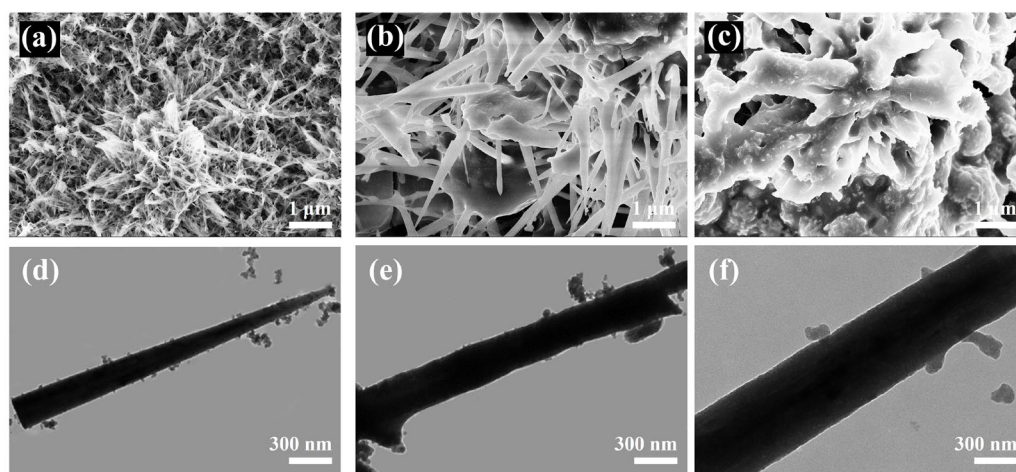


Figure 3. The SEM and TEM images of (a,d) NiCoP@NiCoP/NF-120, (b,e) NiCoP@NiCoP/NF-140 and (c,f) NiCoP@NiCoP/NF-180.

2.1.2. Characterization of Electrochemical Performance

In order to evaluate the catalytic HER activity, the NiCoP@NiCoP/NF was electrochemically tested in 1 M KOH solution ($\text{pH} \approx 14$). Based on a three-electrode system, Pt foil was used as the counter electrode, and Hg/HgO was used as the reference electrode. NiCoP@NiCoP/NF-120, NiCoP@NiCoP/NF-140, NiCoP@NiCoP/NF-160, NiCoP@NiCoP/NF-180, bare NF and Pt/C (20%) electrodes were characterized and compared. The polarization curves recorded by linear sweep voltammetry (LSV) are shown in Figure 4a. All polarization curves have undergone iR compensation. As shown in Figure 4a,c, compared to NiCoP@NiCoP/NF-120 (172 mV), NiCoP@NiCoP/NF-140 (195 mV), NiCoP@NiCoP/NF-180 (351 mV), bare NF (303 mV) and other precursor catalysts, the NiCoP@NiCoP/NF-160 shows the lowest 144 mV overpotential (120 mV for 50 mA cm^{-2}) at the current density of 100 mA cm^{-2} . Benefiting from the modulation of non-metallic P on the electronic structure of Ni and Co d-bands, NiCoP catalysts show a low overpotential in HER. In addition, we also discussed the influence of the amount of sodium hypophosphite on the electrode performance during high-temperature annealing. We investigated the effect of different PH_3 concentrations on the HER performance of NiCoP products by controlling the amount of NaH_2PO_2 added during the phosphating process. At a current density of 50 mA cm^{-2} , the overpotentials of NiCoP@NiCoP/NF-0.2, NiCoP@NiCoP/NF-0.5 and NiCoP@NiCoP/NF-2 are 255, 220 and 149 mV. At a current density of 100 mA cm^{-2} , the overpotentials of NiCoP@NiCoP/NF-0.2, NiCoP@NiCoP/NF-0.5 and NiCoP@NiCoP/NF-2 are 297, 302 and 184 mV (Figure S4a). According to the experimental data, the NiCoP obtained with the reaction of 1 g NaH_2PO_2 has the best HER overpotential. Compared with single-phase NiCoP, the NiCoP-composite structure has an obviously lower overpotential (Figure S1c). The Tafel slope can reflect the kinetic process of the electrode during hydrogen evolution. According to the LSV curve of the samples, they can be directly converted into Tafel curves, and the growth trend of overpotential with current density can be reflected by linear fitting of the specific current density range. The smaller the Tafel slope, the smaller the change in overpotential with increasing current density, and the better the electrocatalytic performance. Additionally, different Tafel slope values indicate different HER rate-determining steps. The smaller the Tafel slope is, the faster the rate-determining step is at the end of the HER double-electron transfer reaction, that is, the Tafel step. As shown in Figure 4b, the Tafel slope of NiCoP@NiCoP/NF-160 (84.2 mV dec^{-1}) is lower than NiCoP@NiCoP/NF-120 (97.5 mV dec^{-1}), NiCoP@NiCoP/NF-140 (96.5 mV dec^{-1}), NiCoP@NiCoP/NF-180 ($336.2 \text{ mV dec}^{-1}$) and NF ($146.4 \text{ mV dec}^{-1}$), while only higher than Pt/C (23.6 mV dec^{-1}), indicating that the HER mechanism of NiCoP@NiCoP/NF-160 is a Volmer–Heyrovsky step, while the HER mechanism of Pt/C is a Volmer–Tafel step, and their rate-determining

steps are the Heyrovsky step and Tafel step, respectively [50]. Similarly, compared to single-phase NiCoP, NiCoP-composite structures also exhibit faster reaction kinetics (Figure S1d). The charge transfer rate of the electrode was further analyzed using electrochemical impedance spectroscopy (EIS). The charge transfer resistance (R_{ct}) is mainly the charge transfer resistance at the interface between the electrode and the electrolyte. A smaller R_{ct} represents better charge transfer ability, which in turn exhibits better catalytic activity. NiCoP@NiCoP/NF-160 had the smallest charge transfer resistance ($R_{ct} \approx 1.17 \Omega$), which is superior to other prepared electrodes, indicating the most advanced charge transfer capability. The effect of different amounts of NaH_2PO_2 on charge transfer was investigated (Figure S4b). Compared with the control samples, NiCoP@NiCoP/NF-160 still had the smallest R_{ct} , which proves that the reduction of overpotential is closely related to the improvement of charge transfer ability.

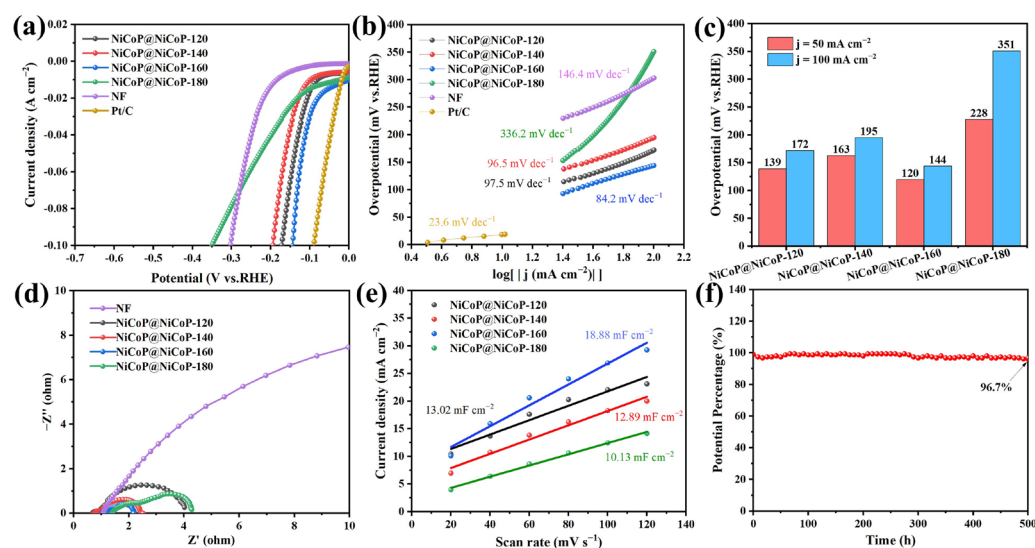


Figure 4. (a) iR-corrected LSV polarization curves, (b) Tafel slope, (c) overpotential at 50 and 100 mA cm^{-2} , (d) EIS plot and (e) ECSA estimated by C_{dl} values of different catalysts. (f) The chronopotentiometry of NiCoP@NiCoP/NF-160 at 100 mA cm^{-2} .

To link structural properties with intrinsic activity, the double-layer capacitance value (C_{dl}) is used to reflect the level of the electrochemical active surface area (ECSA) of the material [51]. The C_{dl} values of different samples were calculated according to cyclic voltammetry (CV). Figure S5 shows the CV curves of NiCoP@NiCoP/NF-120, NiCoP@NiCoP/NF-140, NiCoP@NiCoP/NF-160 and NiCoP@NiCoP/NF-180. Under the voltage range of $-0.725 \sim -0.825$ V vs. Hg/HgO, the polarization current density contrast of the cathode and anode corresponding to the scanning speed and the middle voltage (0.775 V vs. RHE) under different scanning speeds ($\Delta J = j_a - j_c$) is plotted as a linear graph (Figure 4e). Due to the proportional relationship between C_{dl} and ECSA, this can be used to evaluate the active surface area of electrodes. Obviously, the C_{dl} value of NiCoP@NiCoP/NF-160 is the highest (18.88 mF cm^{-2}), higher than NiCoP@NiCoP/NF-120 (13.02 mF cm^{-2}), NiCoP@NiCoP/NF-140 (12.89 mF cm^{-2}) and NiCoP@NiCoP/NF-180 (10.13 mF cm^{-2}). This comparison shows that the appropriate hydrothermal temperature can affect the morphology and structure of the catalyst, expose more active sites and further affect the HER activity of the catalyst. Increased ECSA means more abundant interface and active sites exposure. To investigate the intrinsic activity of catalysts, we performed ECSA normalization on the LSV curves (Figure S6). The results indicate that the NiCoP@NiCoP/NF-160 exhibits higher intrinsic catalytic activity compared to the control samples. Based on the above results, the joint improvement of intrinsic activity, accessible active sites and charge transfer ability leads to a significant decrease in the HER overpotential of the catalyst.

In addition to evaluating the HER activity of the catalyst, the stability of the electrode is also one of the most effective means to determine the application value of the catalyst. Figure 4f shows the trend of electrode potential over time at a current density of 100 mA cm^{-2} . After 500 h of the HER test, the retention rate of electrode HER overpotential is still as high as 96.7% (the potential percentage is obtained from the ratio of initial potential to test potential). The long-term stability of the material is not only attributed to the establishment of the composite structure but may also be related to the small amount of amorphous nickel/cobalt phosphides detected by XRD and XPS characterizations, thereby improving the corrosion resistance of the material. After 500 h of HER testing, we recorded changes in the morphology, phase and catalytic performance of the catalyst. The LSV after the stability test displayed only a small shift (10 mV at 100 mA cm^{-2}) from that at the beginning, which shows that the active sites of the catalyst are well maintained (Figure S7). In addition, the SEM, XRD and TEM results after stability testing showed that after long-term stability testing, the nanosheets grown on the surface tended to become thicker and larger, and the nanowires also showed slight aggregation (Figure 5a–c). However, the original bonding mode was still maintained overall, and the phase of the material did not change, again confirming its good durability. From the XPS spectra after stability, it can also be seen that there is no significant change in the chemical state of the material before and after testing (Figure 5d–f). It is worth noting that the P-Metal peaks appeared in the XPS of P 2p with a significant intensity, which further proved that the absence of P-Metal peaks before testing was caused by surface oxidation of the sample. The improvement of the HER activity of the catalyst is closely related to the number of accessible active sites, the intrinsic activity, the efficiency of charge and mass transfer and the stability displayed by the active substances. After being optimized by temperature and P introduction, the homologous NiCoP/NF catalyst has a more suitable electronic structure, more stable structure characteristics and higher conductivity, thereby demonstrating good HER activity.

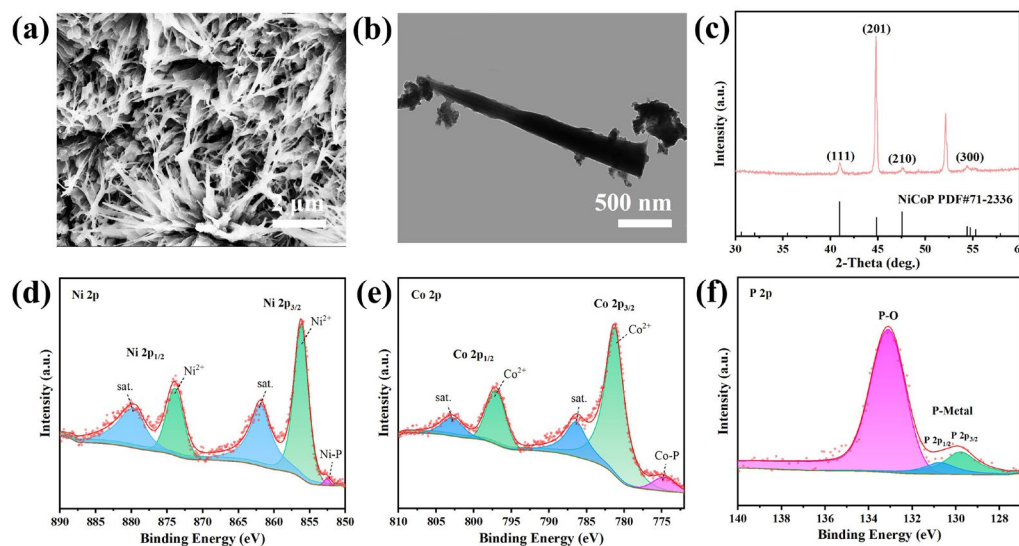


Figure 5. The (a) SEM, (b) TEM, (c) XRD images and (d–f) XPS spectra of NiCoP@NiCoP/NF-160 after 500 h stability test.

3. Materials and Methods

3.1. Materials and Chemicals

The following reagents were obtained and used as received without further processing: nickel(II) nitrate hexahydrate ($\text{Ni}(\text{NO}_3)_2 \cdot 6\text{H}_2\text{O}$, AR, Tianjin Kermel Chemical Reagent Co., Ltd., Tianjin, China), cobalt nitrate hexahydrate ($\text{Co}(\text{NO}_3)_2 \cdot 6\text{H}_2\text{O}$, 99%, Shanghai Aladdin Biochemical Technology Co., Ltd., Shanghai, China), ammonium fluoride (NH_4F , 98%, Shanghai Aladdin Biochemical Technology Co., Ltd., Shanghai, China), urea ($\text{CH}_4\text{N}_2\text{O}$, AR, Tianjin Kermel Chemical Reagent Co., Ltd., Tianjin, China), sodium hypophosphite

($\text{NaH}_2\text{PO}_2 \cdot \text{H}_2\text{O}$, AR, Shanghai Macklin Biochemical Co., Ltd., Shanghai, China), KOH (AR, Tianjin Kermel Chemical Reagent Co., Ltd., Tianjin, China) and commercial Pt/C (20 wt%, Sigma-Aldrich Chemical Reagent Co., Ltd., St. Louis, MO, USA).

3.2. Preparation

3.2.1. Synthesis of NiCo-LDH/NF

Firstly, the nickel foam (1 cm \times 3 cm) was sonicated in 3 M HCl, ethanol and deionized water for 10 min, respectively to remove the surface oxide layer. Then, 1 mmol $\text{Ni}(\text{NO}_3)_2 \cdot 6\text{H}_2\text{O}$, 2 mmol $\text{Co}(\text{NO}_3)_2 \cdot 6\text{H}_2\text{O}$, 6 mmol NH_4F and 6 mmol urea were dissolved in 60 mL deionized water. Magnetic stirring was performed at room temperature for 10 min. Then, they were added together into a 100 mL Teflon stainless steel autoclave to react at 120 °C for 8 h. When the reaction was completed, the sample was taken out and washed alternately with deionized water and ethanol several times and dried under vacuum at 60 °C for 12 h. Finally, NiCo-LDH nanosheets were uniformly grown on the NF.

3.2.2. Synthesis of NiCo-LDH@NiCo-LDH/NF

The as-prepared NiCo-LDH/NF nanosheets were transferred together with 60 mL aqueous solution containing 1 mmol $\text{Ni}(\text{NO}_3)_2 \cdot 6\text{H}_2\text{O}$, 2 mmol $\text{Co}(\text{NO}_3)_2 \cdot 6\text{H}_2\text{O}$ and 6 mmol of urea into a 100 mL Teflon stainless steel autoclave. The mixed solution was maintained at 160 °C for 6 h. The prepared samples were repeatedly washed with ethanol and deionized water several times, and vacuum dried at 60 °C for 12 h. Finally, NiCo-LDH nanowires were grown in situ on NiCo-LDH nanosheet arrays. The obtained samples were named NiCo-LDH@NiCo-LDH/NF-120, NiCo-LDH@NiCo-LDH/NF-140, NiCo-LDH@NiCo-LDH/NF-160 and NiCo-LDH@NiCo-LDH/NF-180 according to the different hydrothermal temperatures.

3.2.3. Synthesis of NiCoP@NiCoP/NF

In the phosphating reaction, the as-prepared NiCo-LDH@NiCo-LDH/NF was placed downstream of the tube furnace and 1 g of $\text{NaH}_2\text{PO}_2 \cdot \text{H}_2\text{O}$ was placed upstream of the Ar atmosphere. Afterwards, we heated the tubular furnace at a heating rate of 2 °C min^{-1} to 300 °C and maintained it for 2 h. After natural cooling and washing, the optimal sample obtained was named NiCoP@NiCoP/NF-160. For comparison, samples obtained at different hydrothermal temperatures were labeled as NiCoP@NiCoP/NF-120, NiCoP@NiCoP/NF-140 and NiCoP@NiCoP/NF-180. In addition, in order to investigate the effect of the amount of P added on the performance of the products, the same method was used to synthesize NiCo-LDH@NiCo-LDH/NF-160, and we changed the dosage of $\text{NaH}_2\text{PO}_2 \cdot \text{H}_2\text{O}$ to 0.2 g, 0.5 g and 2 g, respectively. The control samples prepared were labeled as NiCoP@NiCoP/NF-0.2, NiCoP@NiCoP/NF-0.5 and NiCoP@NiCoP/NF-2. The NiCoP/NF sample was prepared by one-step hydrothermal phosphorization. The precursor preparation of NiCoP nanosheets and NiCoP nanowires is consistent with the first- and second-step hydrothermal methods of NiCoP@NiCoP/NF-160, respectively.

3.3. Materials Characterization

Field emission scanning electron microscopy (FESEM, Carl Zeiss Super55 (Carl Zeiss NTS GmbH, Oberkochen, Germany) operated at 15 kV) was carried out to observe the morphology of samples. Transmission electron microscopy (TEM) images were obtained using a Hitachi HT7700 electron microscope (HITACHI Transmission Electron Microscope, Tokyo, Japan) at 120 kV. The phase composition and crystal structure were characterized by X-ray diffraction (XRD, RigakuSmart Lab, X-ray Diffractometer, Tokyo, Japan) at a scanning rate of 5° min^{-1} . X-ray photoelectron spectroscopy (XPS, ThermoFisher Nexsa, Fanrui Yunzhi Technology (Zhengzhou) Co., Ltd., Zhengzhou, China) was used to analyze the chemical composition and charge transfer of the samples.

3.4. Electrochemical Measurements

All the electrochemical measurements were performed on a CHI 660E electrochemical workstation (CH Instruments, Inc., Shanghai, China) at room temperature. All measurements were performed in 1 M KOH aqueous electrolyte. In a three-electrode system, the final catalyst NiCoP@NiCoP/NF is used as the working electrode directly, with the Hg/HgO electrode and Pt foil as the reference electrode and counter electrode, respectively. Linear sweep voltammetry (LSV) curves were measured at a scanning speed of 5 mV s^{-1} and iR correction was performed on the obtained results. Electrochemical impedance spectroscopy (EIS) data collection was performed in the frequency range of 100 kHz to 0.01 Hz with an AC voltage of 5 mV. The double-layer capacitance of the electrode was characterized by cyclic voltammetry (CV) and tested at different scan rates from 20 to 120 mV s^{-1} in the potential region of $-0.725 \sim -0.825 \text{ V}$. The chronopotentiometry was used for long-term stability testing at a constant current density of 100 mA cm^{-2} . All potentials reported in our work were displayed vs. the reversible hydrogen electrode (RHE) according to the equation $E_{(\text{RHE})} = E_{(\text{Hg}/\text{HgO}/\text{OH}^-)} + 0.925 \text{ V}$. $\text{ECSA} = C_{\text{dl}}/C_s$, in which C_s is the specific capacitance for a flat surface and is taken as $60 \mu\text{F cm}^{-2}$ in alkaline electrolytes.

4. Conclusions

The hierarchical construction of different components with homologous structures can not only fully utilize the intrinsic activity of materials, but can also improve the chemical stability of synergistic components, thereby promoting the effective progress of HER. This work investigates the coupling construction of different morphological structures on NF substrates, and achieves the construction of higher active phases through anion exchange between P^{3-} and OH^- . Based on the regulation of hydrothermal temperature and non-metallic introduction, a well-designed hierarchical structure and fully exposed active sites are fully combined. By using the synergistic catalysis of NiCo bimetallic sites in HER and the regulation of P on the electronic structure of NiCo, the synthesized NiCoP@NiCoP/NF-160 has rich catalytic sites, rich diffusion channels and low charge transfer resistance. Even at a current density of 100 mA cm^{-2} , the catalyst still exhibits HER stability for over 500 h, and its morphology, structure and catalytic activity remain unchanged. This provides a reference scheme for the application of the ion exchange method and the construction of a hierarchical structure.

Supplementary Materials: The following supporting information can be downloaded at: <https://www.mdpi.com/article/10.3390/catal13091232/s1>, Figure S1: SEM images of (a) NiCoP nanosheets and (b) NiCoP nanowires. (c) LSV curves and (d) Tafel plots of NiCoP nanosheets and NiCoP nanowires; Figure S2: XRD spectra of NiCoP@NiCoP/NF-120, NiCoP@NiCoP/NF-140, NiCoP@NiCoP/NF-160 and NiCoP@NiCoP/NF-180; Figure S3: XPS survey spectra of NiCoP/NF; Figure S4: (a) iR-corrected LSV polarization curves and (b) EIS plot of NiCoP@NiCoP/NF-0.2, NiCoP@NiCoP/NF-0.5 and NiCoP@NiCoP/NF-2; Figure S5: CV curves of (a) NiCoP@NiCoP/NF-120, (b) NiCoP@NiCoP/NF-140, (c) NiCoP@NiCoP/NF-160 and (d) NiCoP@NiCoP/NF-180; Figure S6: ECSA-normalized polarization curves of NiCoP@NiCoP/NF-120, NiCoP@NiCoP/NF-140, NiCoP@NiCoP/NF-160 and NiCoP@NiCoP/NF-180; Figure S7: LSV curves of NiCoP@NiCoP/NF-160 before and after the stability test.

Author Contributions: Conceptualization, A.S. and G.S.; methodology, S.S. and L.B.; validation, M.D. and L.B.; formal analysis, S.S.; investigation, S.S.; data curation, S.S. and M.D.; writing—original draft preparation, S.S.; writing—review and editing, A.S., L.W. and H.D.; resources, A.S. and G.S.; supervision, X.Q. All authors have read and agreed to the published version of the manuscript.

Funding: This work was financially supported by the Hebei Province Natural Science Foundation Innovation Group Project (B2021203016), the National Natural Science Foundation of China (52174281), the Subsidy for Hebei Key Laboratory of Applied Chemistry after Operation Performance (22567616H), the Funding from the Hebei Provincial Department of Human Resources and Social Security (C20230328) and the Yanshan University (8190410), the Doctoral Scientific Research Foun-

dition of Shijiazhuang University (20BS001) and the Science and Technology Research Project of Colleges and Universities in Hebei Province (Z2020127).

Data Availability Statement: The data that support the findings of this study are available from the corresponding author upon reasonable request.

Acknowledgments: We would like to thank Fanrui Yunzhi Technology (Zhengzhou) Co., Ltd. for the XPS measurement.

Conflicts of Interest: The authors declare no conflict of interest.

References

1. Zou, X.; Zhang, Y. Noble metal-free hydrogen evolution catalysts for water splitting. *Chem. Soc. Rev.* **2015**, *44*, 5148. [[CrossRef](#)] [[PubMed](#)]
2. Adam, A.; Suliman, M.H.; Siddiqui, M.N.; Yamani, Z.H.; Merzougui, B.; Qamar, M. Interconnected Hollow Cobalt Phosphide Grown on Carbon Nanotubes for Hydrogen Evolution Reaction. *ACS Appl. Mater. Interfaces* **2018**, *10*, 29407. [[CrossRef](#)] [[PubMed](#)]
3. Cao, H.; Xie, Y.; Wang, H.; Xiao, F.; Wu, A.; Li, L.; Xu, Z.; Xiong, N.; Pan, K. Flower-like CoP microballs assembled with (002) facet nanowires via precursor route: Efficient electrocatalysts for hydrogen and oxygen evolution. *Electrochim. Acta* **2018**, *259*, 830. [[CrossRef](#)]
4. Zhan, Z.; Gao, P.; Lei, T.; Zhang, S.; Du, Y. N-, Se-, and S-Doped Bimetallic NiCoP Nanosheet Arrays as Efficient Hydrogen Evolution Electrocatalysts. *ACS Sustain. Chem. Eng.* **2023**, *11*, 4980. [[CrossRef](#)]
5. Wei, D.; Chen, L.; Tian, L.; Ramakrishna, S.; Ji, D. Hierarchically Structured CoNiP/CoNi Nanoparticle/Graphene/Carbon Foams as Effective Bifunctional Electrocatalysts for HER and OER. *Ind. Eng. Chem. Res.* **2023**, *62*, 4987. [[CrossRef](#)]
6. Yang, L.; Yang, T.; Wang, E.; Yu, X.; Wang, K.; Du, Z.; Cao, S.; Chou, K.-C.; Hou, X. Bifunctional hierarchical NiCoP@FeNi LDH nanosheet array electrocatalyst for industrial-scale high-current-density water splitting. *J. Mater. Sci. Technol.* **2023**, *159*, 33. [[CrossRef](#)]
7. Deng, Y.; Cao, Y.; Xia, Y.; Xi, X.; Wang, Y.; Jiang, W.; Yang, D.; Dong, A.; Li, T. Self-Templated Synthesis of CoFeP@C Cage-In-Cage Superlattices for Enhanced Electrocatalytic Water Splitting. *Adv. Energy Mater.* **2022**, *12*, 2202394. [[CrossRef](#)]
8. Li, A.; Zhang, L.; Wang, F.; Zhang, L.; Li, L.; Chen, H.; Wei, Z. Rational design of porous Ni-Co-Fe ternary metal phosphides nanobricks as bifunctional electrocatalysts for efficient overall water splitting. *Appl. Catal. B Environ.* **2022**, *310*, 121353. [[CrossRef](#)]
9. Lin, J.; Yan, Y.; Li, C.; Si, X.; Wang, H.; Qi, J.; Cao, J.; Zhong, Z.; Fei, W.; Feng, J. Bifunctional Electrocatalysts Based on Mo-Doped NiCoP Nanosheet Arrays for Overall Water Splitting. *Nano Micro Lett.* **2019**, *11*, 55. [[CrossRef](#)]
10. Li, J.; Hu, Y.; Huang, X.; Zhu, Y.; Wang, D. Bimetallic Phosphide Heterostructure Coupled with Ultrathin Carbon Layer Boosting Overall Alkaline Water and Seawater Splitting. *Small* **2023**, *19*, e2206533. [[CrossRef](#)]
11. Wang, P.; Luo, Y.; Zhang, G.; Wu, M.; Chen, Z.; Sun, S.; Shi, Z. MnO_x-Decorated Nickel-Iron Phosphides Nanosheets: Interface Modifications for Robust Overall Water Splitting at Ultra-High Current Densities. *Small* **2022**, *18*, e2105803. [[CrossRef](#)] [[PubMed](#)]
12. Zhang, X.; Zhang, B.; De Luna, P.; Liang, Y.; Comin, R.; Voznyy, O.; Han, L.; Garcia de Arquer, F.P.; Liu, M.; Dinh, C.T.; et al. Theory-driven design of high-valence metal sites for water oxidation confirmed using in situ soft X-ray absorption. *Nat. Chem.* **2018**, *10*, 149. [[CrossRef](#)] [[PubMed](#)]
13. Hu, X.; Fan, J.; Wang, R.; Li, M.; Sun, S.; Xu, C.; Pan, F. Vacancies and interfaces engineering of core-shell heterostructured NiCoP/NiO as trifunctional electrocatalysts for overall water splitting and zinc-air batteries. *Green Energy Environ.* **2023**, *8*, 601. [[CrossRef](#)]
14. Qi, Y.; Zhang, L.; Sun, L.; Chen, G.; Luo, Q.; Xin, H.; Peng, J.; Li, Y.; Ma, F. Sulfur doping enhanced desorption of intermediates on NiCoP for efficient alkaline hydrogen evolution. *Nanoscale* **2020**, *12*, 1985. [[CrossRef](#)] [[PubMed](#)]
15. Wang, D.; Zhang, Y.; Fei, T.; Mao, C.; Song, Y.; Zhou, Y.; Dong, G. NiCoP/NF 1D/2D Biomimetic Architecture for Markedly Enhanced Overall Water Splitting. *ChemElectroChem* **2021**, *8*, 3064. [[CrossRef](#)]
16. Zhang, X.; Li, Y.; Wu, Z.; Sheng, H.; Hu, Y.; Li, C.; Li, H.; Cao, L.; Dong, B. Crystalline/amorphous composite interface induced by NaBH₄ hydrolysis reaction: A new interfacial electrocatalyst for efficient oxygen evolution reaction. *Mater. Today Energy* **2022**, *26*, 100987. [[CrossRef](#)]
17. Chen, D.; Lu, R.; Pu, Z.; Zhu, J.; Li, H.-W.; Liu, F.; Hu, S.; Luo, X.; Wu, J.; Zhao, Y.; et al. Ru-doped 3D flower-like bimetallic phosphide with a climbing effect on overall water splitting. *Appl. Catal. B Environ.* **2020**, *279*, 119396. [[CrossRef](#)]
18. Ding, X.; Pei, L.; Huang, Y.; Chen, D.; Xie, Z. Hollow NiCoP Nanoprisms Derived from Prussian Blue Analogues as Bifunctional Electrocatalysts for Urea-Assisted Hydrogen Production in Alkaline Media. *Small* **2022**, *18*, e2205547. [[CrossRef](#)]
19. Jiang, N.; Shi, S.J.; Cui, Y.Y.; Jiang, B.L. The effect of calcination temperature on the hydrogen evolution reaction performance of Co/NiCoP nano-heterojunction. *J. Alloys Compd.* **2022**, *929*, 167229. [[CrossRef](#)]
20. Tiwari, A.P.; Lee, K.; Kim, K.; Kim, J.; Novak, T.G.; Jeon, S. Conformally Coated Nickel Phosphide on 3D, Ordered Nanoporous Nickel for Highly Active and Durable Hydrogen Evolution. *ACS Sustain. Chem. Eng.* **2020**, *8*, 17116. [[CrossRef](#)]
21. Tiwari, A.P.; Bae, G.; Yoon, Y.; Kim, K.; Kim, J.; Lee, Y.-L.; An, K.-S.; Jeon, S. Chemical Strain Engineering of Copper Atoms on Continuous Three-Dimensional-Nanopatterned Nickel Nitride to Accelerate Alkaline Hydrogen Evolution. *ACS Sustain. Chem. Eng.* **2023**, *11*, 5229. [[CrossRef](#)]

22. Li, W.; Cheng, G.; Peng, S.; Sun, M.; Wang, S.; Han, S.; Liu, Y.; Zhai, T.; Yu, L. Tuning hydrogen binding energy by interfacial charge transfer enables pH-universal hydrogen evolution catalysis of metal phosphides. *Chem. Eng. J.* **2022**, *430*, 132699. [[CrossRef](#)]
23. Liu, Y.; Feng, Q.; Liu, W.; Li, Q.; Wang, Y.; Liu, B.; Zheng, L.; Wang, W.; Huang, L.; Chen, L.; et al. Boosting interfacial charge transfer for alkaline hydrogen evolution via rational interior Se modification. *Nano Energy* **2021**, *81*, 105641. [[CrossRef](#)]
24. Shi, J.; Peng, W.; Yang, Y.F.; Li, B.; Nie, J.; Wan, H.; Li, Y.; Huang, G.F.; Hu, W.; Huang, W.Q. A General Strategy for Synthesis of Binary Transition Metal Phosphides Hollow Sandwich Heterostructures. *Small* **2023**, *19*, 2302906. [[CrossRef](#)] [[PubMed](#)]
25. Niu, H.J.; Yan, Y.; Jiang, S.; Liu, T.; Sun, T.; Zhou, W.; Guo, L.; Li, J. Interfaces Decrease the Alkaline Hydrogen-Evolution Kinetics Energy Barrier on NiCoP/Ti₃C₂T_x MXene. *ACS Nano* **2022**, *16*, 11049. [[CrossRef](#)] [[PubMed](#)]
26. Wang, J.; Yang, A.; Li, J.; Su, K.; Tang, Y.; Qiu, X. Top-down and facet-selective phase-segregation to construct concave nanocages with strongly coupled hetero-interface for oxygen evolution reaction. *Appl. Catal. B Environ.* **2022**, *300*, 120727. [[CrossRef](#)]
27. Yang, H.; Guo, P.; Wang, R.; Chen, Z.; Xu, H.; Pan, H.; Sun, D.; Fang, F.; Wu, R. Sequential Phase Conversion-Induced Phosphides Heteronanorod Arrays for Superior Hydrogen Evolution Performance to Pt in Wide pH Media. *Adv. Mater.* **2022**, *34*, e2107548. [[CrossRef](#)] [[PubMed](#)]
28. Lei, X.; Ge, S.; Tan, Y.; Wang, Z.; Li, J.; Li, X.; Hu, G.; Zhu, X.; Huang, M.; Zhu, Y.; et al. High Capacity and Energy Density of Zn-Ni-Co-P Nanowire Arrays as an Advanced Electrode for Aqueous Asymmetric Supercapacitor. *ACS Appl. Mater. Interfaces* **2020**, *12*, 9158. [[CrossRef](#)]
29. Li, L.; Zou, W.; Ye, Q.; Li, Q.; Feng, Q.; Wei, J.; Xu, X.; Wang, F. Quasi-parallel nickel cobalt phosphide nanosheet arrays as highly efficient electrocatalyst for hydrogen evolution and overall water splitting at large current densities. *J. Power Sources* **2021**, *516*, 230657. [[CrossRef](#)]
30. Tong, X.; Liao, W.; Zhai, Y.; Liu, P.; Yang, Q.; Chen, T. NiO/Co₂P Nanosheets with Heterogeneous Structure as a Multifunctional Catalyst for Overall Water Splitting. *J. Electrochem. Soc.* **2023**, *170*, 063509. [[CrossRef](#)]
31. Yu, W.; Sun, L.; Huo, L.; Zhao, H. Synergistic Coupling of CoFe-LDH Nanosheets with Cu₃P Nanoarrays for Efficient Water Splitting. *ACS Appl. Energy Mater.* **2023**, *6*, 5548. [[CrossRef](#)]
32. Ding, Z.; Yu, H.; Liu, X.; He, N.; Chen, X.; Li, H.; Wang, M.; Yamauchi, Y.; Xu, X.; Amin, M.A.; et al. Prussian blue analogue derived cobalt-nickel phosphide/carbon nanotube composite as electrocatalyst for efficient and stable hydrogen evolution reaction in wide-pH environment. *J. Colloid Interface Sci.* **2022**, *616*, 210. [[CrossRef](#)] [[PubMed](#)]
33. Yan, L.; Cao, L.; Dai, P.; Gu, X.; Liu, D.; Li, L.; Wang, Y.; Zhao, X. Metal-Organic Frameworks Derived Nanotube of Nickel-Cobalt Bimetal Phosphides as Highly Efficient Electrocatalysts for Overall Water Splitting. *Adv. Funct. Mater.* **2017**, *27*, 1703455. [[CrossRef](#)]
34. Zhou, X.; Fei, F.; Li, M.; Cao, X.; Dong, X.; Li, L.; Yuan, N.; Ding, J. Electrochemically Oxidized Aligned Carbon Nanotube Arrays Embedding Foam Substrates for Water Splitting. *ACS Appl. Nano Mater.* **2023**, *6*, 8028. [[CrossRef](#)]
35. Yue, Z.; Yao, S.; Li, Y.; Zhu, W.; Zhang, W.; Wang, R.; Wang, J.; Huang, L.; Zhao, D.; Wang, J. Surface engineering of hierarchical Ni(OH)₂ nanosheet@nanowire configuration toward superior urea electrolysis. *Electrochim. Acta* **2018**, *268*, 211. [[CrossRef](#)]
36. Zheng, X.; Peng, Y.; Xu, S.; Huang, L.; Liu, Y.; Li, D.; Zhu, J.; Jiang, D. NiCoP-nanocubes-decorated CoSe₂ nanowire arrays as high-performance electrocatalysts toward oxygen evolution reaction. *J. Colloid Interface Sci.* **2023**, *648*, 141. [[CrossRef](#)] [[PubMed](#)]
37. Han, A.; Chen, H.; Zhang, H.; Sun, Z.; Du, P. Ternary metal phosphide nanosheets as a highly efficient electrocatalyst for water reduction to hydrogen over a wide pH range from 0 to 14. *J. Mater. Chem. A* **2016**, *4*, 10195. [[CrossRef](#)]
38. Jiang, D.; Xu, Y.; Yang, R.; Li, D.; Meng, S.; Chen, M. CoP₃/CoMoP Heterogeneous Nanosheet Arrays as Robust Electrocatalyst for pH-Universal Hydrogen Evolution Reaction. *ACS Sustain. Chem. Eng.* **2019**, *7*, 9309. [[CrossRef](#)]
39. Wang, X.; Yu, X.; Bai, J.; Yuan, G.; He, P.; Zhu, Y.; Wu, S.; Qin, F.; Ren, L. Interface engineering assisted Fe-Ni₃S₂/Ni₂P heterostructure as a high-performance bifunctional electrocatalyst for OER and HER. *Electrochim. Acta* **2023**, *458*, 142524. [[CrossRef](#)]
40. Li, S.; Wang, Y.; Peng, S.; Zhang, L.; Al-Enizi, A.M.; Zhang, H.; Sun, X.; Zheng, G. Co-Ni-Based Nanotubes/Nanosheets as Efficient Water Splitting Electrocatalysts. *Adv. Energy Mater.* **2016**, *6*, 1501661. [[CrossRef](#)]
41. Bai, L.; Song, A.; Lei, X.; Zhang, T.; Song, S.; Tian, H.; Liu, H.; Qin, X.; Wang, G.; Shao, G. Hierarchical construction of hollow NiCo₂S₄ nanotube@NiCo₂S₄ nanosheet arrays on Ni foam as an efficient and durable electrocatalyst for hydrogen evolution reaction. *Int. J. Hydrog. Energy* **2022**, *47*, 38524. [[CrossRef](#)]
42. Chen, L.; Song, Y.; Liu, Y.; Xu, L.; Qin, J.; Lei, Y.; Tang, Y. NiCoP nanoleaves array for electrocatalytic alkaline H₂ evolution and overall water splitting. *J. Energy Chem.* **2020**, *50*, 395. [[CrossRef](#)]
43. Fang, Z.; Peng, L.; Qian, Y.; Zhang, X.; Xie, Y.; Cha, J.J.; Yu, G. Dual Tuning of Ni-Co-A (A = P, Se, O) Nanosheets by Anion Substitution and Holey Engineering for Efficient Hydrogen Evolution. *J. Am. Chem. Soc.* **2018**, *140*, 5241. [[CrossRef](#)] [[PubMed](#)]
44. Lv, X.; Li, X.; Yang, C.; Ding, X.; Zhang, Y.; Zheng, Y.Z.; Li, S.; Sun, X.; Tao, X. Large-Size, Porous, Ultrathin NiCoP Nanosheets for Efficient Electro/Photocatalytic Water Splitting. *Adv. Funct. Mater.* **2020**, *30*, 1910830. [[CrossRef](#)]
45. Lu, Y.; Liu, C.; Xu, S.; Liu, Y.; Jiang, D.; Zhu, J. Facile synthesis of hierarchical NiCoP nanosheets/NiCoP nanocubes homojunction electrocatalyst for highly efficient and stable hydrogen evolution reaction. *Appl. Surf. Sci.* **2021**, *565*, 150537. [[CrossRef](#)]
46. Guo, J.; Zhan, Z.; Lei, T.; Yin, P. Facile synthesis of self-supported intertwined columnar NiCoP as a high efficient electrocatalyst for hydrogen evolution reaction. *Int. J. Hydrog. Energy* **2022**, *47*, 5974. [[CrossRef](#)]
47. Wu, H.; Liu, P.; Yin, M.; Hou, Z.; Hu, L.; Dang, J. Surface modification engineering on three-dimensional self-supported NiCoP to construct NiCoO_x/NiCoP for highly efficient alkaline hydrogen evolution reaction. *J. Alloys Compd.* **2020**, *835*, 155364. [[CrossRef](#)]

48. Wang, Z.; Chen, J.; Song, E.; Wang, N.; Dong, J.; Zhang, X.; Ajayan, P.M.; Yao, W.; Wang, C.; Liu, J.; et al. Manipulation on active electronic states of metastable phase beta-NiMoO₄ for large current density hydrogen evolution. *Nat. Commun.* **2021**, *12*, 5960. [[CrossRef](#)]
49. Geng, L.; Liu, Q.; Chen, J.; Jia, P.; Ye, H.; Yan, J.; Zhang, L.; Tang, Y.; Huang, J. In situ observation of electrochemical Ostwald ripening during sodium deposition. *Nano Res.* **2021**, *15*, 2650. [[CrossRef](#)]
50. Guo, Y.; Park, T.; Yi, J.W.; Henzie, J.; Kim, J.; Wang, Z.; Jiang, B.; Bando, Y.; Sugahara, Y.; Tang, J.; et al. Nanoarchitectonics for Transition-Metal-Sulfide-Based Electrocatalysts for Water Splitting. *Adv. Mater.* **2019**, *31*, e1807134. [[CrossRef](#)]
51. Zhao, G.; Rui, K.; Dou, S.X.; Sun, W. Heterostructures for Electrochemical Hydrogen Evolution Reaction: A Review. *Adv. Funct. Mater.* **2018**, *28*, 1803291. [[CrossRef](#)]

Disclaimer/Publisher's Note: The statements, opinions and data contained in all publications are solely those of the individual author(s) and contributor(s) and not of MDPI and/or the editor(s). MDPI and/or the editor(s) disclaim responsibility for any injury to people or property resulting from any ideas, methods, instructions or products referred to in the content.